CHAPTER 6

An Algorithm of Rotation Invariant Texture Classification

6.1. Introduction

Many texture classification schemes have been presented that are invariant to image rotation so far. The major existing approaches include image rotation invariant statistical features, moment invariants, polarogram features, Hough transform features, iso-energy directional signatures in 2D Fourier spectra, autoregressive models, Gaussian Markov random field models, multi-channel filtering and wavelet transforms. Details can be found in *Chapter 2*.

Image rotation invariant classifiers normally derive their features directly from a single image and are tested using rotated images. If the image texture results solely from albedo variation rather that surface relief or if the illumination is not directional or immediately overhead, then these schemes are surface-rotation invariant as well. However, in many cases rotation of a textured surface produces images that differ radically from those provided by pure image rotation (see *Figure 6. 1*). These images show that rotation of a 3D surface texture does not result in a simple rotation of the image texture. This is mainly due to the directional filtering effect of imaging using side-lighting [Chantler94a, Chantler94b]. Such changes in appearance can cause significant failures in image-base texture classifiers. For instance a rotation of *90°* of the illuminant tilt angle can cause the mis-classification rate of a texture classifier to change from *4-5%* to nearly *100%* [Chantler94a]. In another way, rotation of the physical texture surface under fixed illumination conditions can also cause significant changes to its appearance. It causes failure of classifiers designed to cope with image rotation as well [McGunigle98].

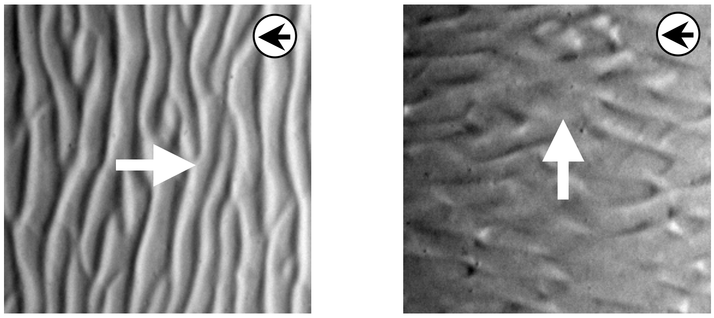

φ = 0° φ = 90°

Figure 6. 1 Two images of the same directional 3D rotated surface texture with identical illuminant. The surface has been rotated through of 0º and 90º (indicated by the white arrows in the centre). The illuminant tilt is kept constant at τ=0° (indicated by the black arrows in white circles).

In this chapter, we present a novel *surface rotation invariant* approach to texture classification. Our approach uses polarograms [Davis81] derived from surface derivative spectra. We use photometric stereo to obtain the required partial derivative fields. They are Fourier transformed and combined to provide a frequency domain function that does not contain the directional artefacts associated with partial derivatives. Polarograms of this function are compared with those of training classes using a goodness-of-fit measure to provide rotation invariant texture classification.

6.2. Surface Rotation-Invariant Texture Features

In previous chapters, we have discussed that we can successfully obtain surface properties using photometric stereo and we will use these 3D surface properties in image properties for classification. The next step is to derive surface rotation-invariant texture features from 3D surface properties that have the ability to provide discrimination between texture classes.

6.2.1 Related Work

As previously stated in *Chapter 2* many texture classification schemes have been presented that are invariant to image rotation [Port97] [Cohen91] [Mao92]. Few take into account the problems caused by illumination described in *Figure 6. 1*. Exceptions include Leung and Malik's classification system which is trained on textures that are each imaged under 20 different illumination and orientation conditions [Leung99]. This generalises the classifier but does not use explicit 3D surface texture information directly; Dana and Nayer describe histogram and correlation model for 3D surface texture and suggest how this might be used to provide a 3D surface texture feature, correlation length [Dana99a]; McGunnigle and Chantler proposed a model-based scheme that used photometric stereo to obtain gradient information [McGunnigle97]. Smith also uses 3D surface texture information directly [Smith99a]. He uses photometric stereo to acquire surface gradient information and suggests the use of features derived from the gradient space. More details about above methods can be recalled in *Chapter 2*.

6.2.2 Development of Features in Frequency Domain

Chantler [Chantler94a] notes that both the directional characteristics and the variance of images of three-dimensional textures can be affected by changing the illumination vector. A frequency domain model based on Kube and Pentland's illumination model is presented and the results of simulations and laboratory experiments allow it to be evaluated. Moreover the model is further developed using empirical data and the resulting model used to design a set of tilt-compensation filters. These filters are used to pre-process images to reduce the effects of changes in the angle of tilt of the illumination (see *Figure 6. 2*).

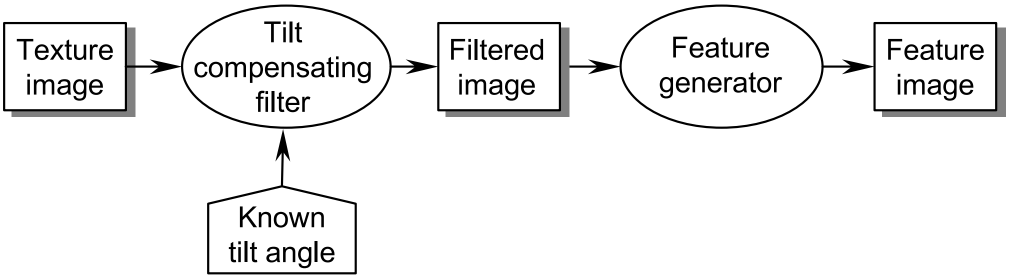

Figure 6. 2 Chantler's frequency domain compensation model for illuminant tilt variation

The classifier is trained under a set of illumination conditions but it is used with arbitrary tilt angles. Application of the filters to the test image set reduced the classification tilt-related errors associated with directional textures only. His method is a simple implementation and avoids high training requirements; however, the illuminant tilt angle has to be known during both the training and classification process. In addition, we have to consider two aspects of illumination conditions: not only tilt angle but also slant angle variations, but he did not give a frequency domain slant compensation scheme. Finally, this single image scheme is not able to estimate signal components perpendicular to the illuminant direction due to the linearization inherent in Kube and Pentland's model.

McGunnigle [McGunnigle98] states that a technique which uses a representation of the physical surface as the basis for the generation of appropriate training data is appropriate. The surface derivative fields of the training surface are estimated using photometric techniques. This allows him to recover surface intrinsic characteristics from several images of the same surface taken at different illumination conditions. A rendering algorithm uses these estimates to simulate the appearance of the training surface when it is illuminated form an arbitrary direction. It is shown that where illuminant direction is varied this system is able to perform significantly better than a naive classifier, and in some cases approaches the level of accuracy obtained from training the classifier under the conditions at which classification is performed.

The scheme was not rotation invariant. Later he proposed another photometric-based system, which is outlined in *Figure 6. 3*. This time, however, the gradient information was directly filtered using isotropic Gabor filters to provide a rotation insensitive scheme [McGunnigle99a]. The filtered derivative fields $p_g(x,y)$ and $q_g(x,y)$ still contain the artefacts of directionality due to the differentiation. As they are only interested in the amount of energy contained in each frequency band, the post-processing stage of the norm function can be non-linear. The resulting quantity is free of the directional filtering effect. A filter approach is adopted to estimate the magnitude and followed by a low-pass filter. Finally, his classification is performed by the statistical discriminated maximum likelihood method.

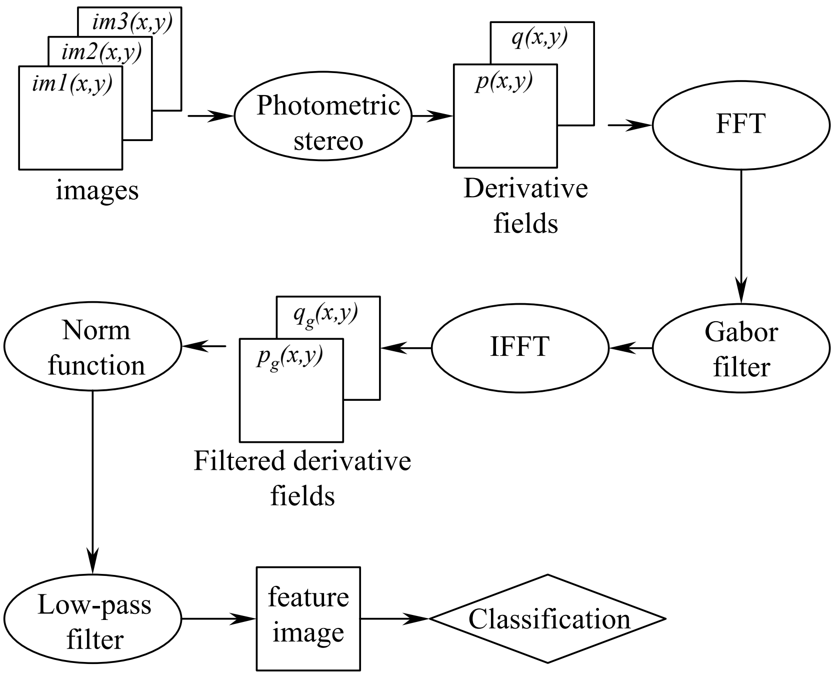

Figure 6. 3 McGunnigle's surface rotation invariant classification scheme

In his scheme, firstly we note that he only use three images to estimate surface derivatives and ignores the shadowing effect. However, in general the shadowing will play an important role in the photometric stereo techniques. Secondly, he assumes that the surface is of approximately Lambertian reflectance and uniform albedo. He does not use any albedo information in his classifier, although albedo information can be isolated from the training data sets. Thirdly, his classification is only performed on the variations in illuminant tilt and the slant angle is kept constant. The effect of slant variation will also have a significant effect on photometric stereo techniques applied to 3D rough surface.

Quivy [Quivy98] presents a look-up table for CFFT based texture classification (see *Figure 6. 4*). The non-linear mapping between image irradiance and surface orientation is represented in a look-up table. He used a calibration object of known shape to generate data mapping the measured brightness values to the corresponding gradient. He then obtained the spectra of the texture gradient by applying a Complex Fast Fourier Transformation (CFFT) to the complex gradient combination $p(x.y)+\boldsymbol{j}\bullet q(x,y)$. Finally, the classification is performed on the maximum of the normalised correlation coefficient between the featured test images and training images. He has to estimate the surface orientation angle by rotating one of the spectra images before comparing the data for classification purposes. Hence this scheme is computationally expensive. On the other hand, the classification accuracy is heavily dependent on the accuracy of the estimated rotation angle. In this circumstance, he reports that an isotropic texture could lead to potential misclassification due to failure of the angle estimation processing.

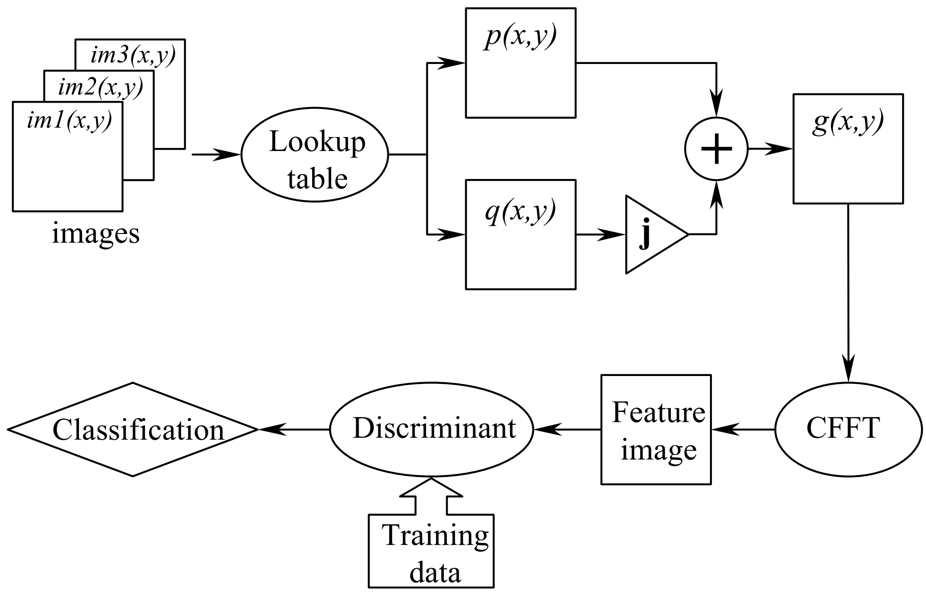

Figure 6. 4 Quivy's lookup table and CFFT based texture classification

Damoiseau [Damoiseau97] developed a correlation method based on polar spectra. She investigated its performance using a set of twenty Brodatz textures (see *Figure 6. 5*). Using multiple frequency ranges on the polar spectra enabled estimation of surface orientation angles more accurately. The overlapping range defined on the frequency range also improves the accuracy of the classifier, although they are all based on the same classification principal. The classification is based on features defined to be the maximum value of the cross-correlation between the polar spectra of the test sample and that of each training sample. We note that Damoiseau's method is based on image data rather than on surface data and the location of the frequency ranges appears to be a very sensitive parameter.

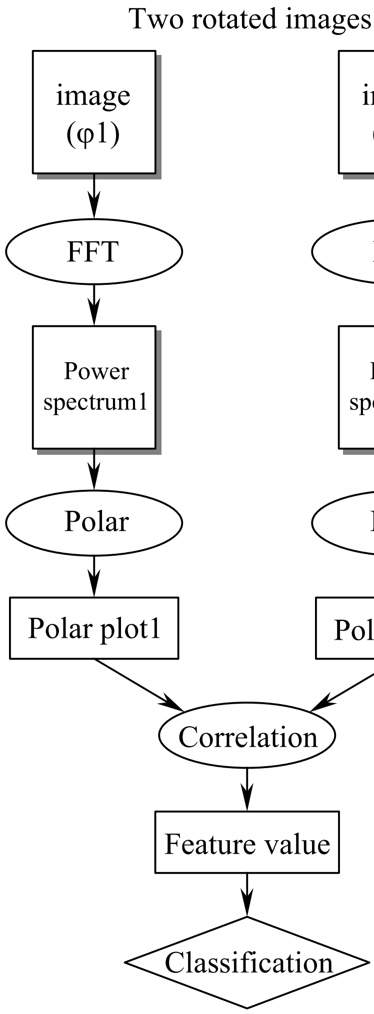

Figure 6. 5   Damoiseau's classification scheme using polar plot and correlation

In general, Chantler's single image scheme [Chantler94a] only gave a frequency domain tilt compensation but slant compensation, and it also share the significant weakness that stems from the linearisation inherent in Kube's model [McGunnigle98]. In McGunnigle's method [McGunnigle98], he ignored the effect of shadowing and kept the surface albedo and slant angle constant in his experiments.

Quivy's method [Quivy98] is computationally expensive and heavily dependent on the accuracy of the estimated rotation angle, which results in the potential misclassification for an isotropic texture. Although the computation in Damoiseau's method [Damoiseau97] is not expensive, it is based on image data but surface data. Therefore, we develop our surface rotation invariant texture classification scheme using photometric stereo.

6.3. Photometric Stereo in Frequency Domain Dual

The aim of this chapter is to develop an algorithm of rotation invariant texture classification for 3D surfaces, so the directional effects which come from the illuminant conditions must be removed before the classification. In this section, we will discuss two of the difficulties in photometric stereo and how we remove the directional artefacts in the frequency domain. Finally we evaluate our algorithm on four synthetic textures and four real textures.

6.3.1 Difficulties in Photometric Stereo

As discussed earlier, we have to use the basic surface properties of the surface rather than the image intensity properties in order to eliminate the effects of illumination and enable the classifier to be robust to the surface rotation. We obtain the partial derivatives of the surface height function using photometric stereo, in which several images of the same surface are taken under different illumination conditions. The photometric stereo method enables us to estimate surface shape. It requires only one camera with a movable light source and can be easily implemented without extra cost in computation. In addition, there is no assumption of smoothness of the 3D surface as required in most single image shape from shading algorithms. We note, however, that there are two main difficulties associated with the surface derivatives:

1. The first is that the surface derivatives are vectors rather than scalar quantities. We will have to use these two surface derivatives together in classifier, rather than one scalar quantity. Recovery of the surface height map by integrating the surface derivatives may yield a scalar field which can be directly incorporated into an existing classifier. However the integration error may be well increase via accumulation.

2. The other difficulty is that there is a direction-related factor, which is an artefact of the partial derivative operator. In this case, this directionality component should be removed before classification.

These two difficulties mean that the partial derivatives of the surface cannot be used directly in a rotation invariant classifier; they must be processed first.

6.3.2 Frequency Domain Dual

This section proposes a method by which the partial derivatives may be combined in the frequency domain in such a way as to remove these directional artefacts. The surface gradient estimations provided by photometric stereo are normally in the form of the partial derivative fields *p(x,y)* and *q(x,y)*.

$$p(x,y) = \partial z(x,y)/\partial x \qquad (6.1)$$

$$q(x,y) = \partial z(x,y)/\partial y \qquad (6.2)$$

where *z(x, y)* is the surface height function of a texture in the *x-y* plane,

and *p(x,y)* and *q(x,y)* are surface partial derivative fields along the *x* direction and *y* direction respectively.

The Fourier transforms of equation (6. 1) and (6. 2) are:

$$P(u,v) = iuS(u,v) = i\omega(\cos\theta)\, S(\omega,\theta) \qquad (6.3)$$

$$Q(u,v) = ivS(u,v) = i\omega(\sin\theta)\, S(\omega,\theta) \qquad (6.4)$$

where $S(u,v)$ and $S(\omega,\theta)$ are the surface magnitude spectrum in its Cartesian and polar forms,

u,v are spatial frequency variables,

and ω,θ are their polar equivalents.

$P(u,v)$ and $Q(u,v)$ are the Fourier transforms of $p(x,y)$ and $q(x,y)$ respectively.

Now equation (6. 3) and (6. 4) show that both derivatives act as directional filters due to the $\cos\theta$ and $\sin\theta$ terms. In particular the partial derivative of a surface rotated by φ is not simply a rotation of the original partial derivative, i.e.

$$P_{\varphi}(\omega,\theta) = i\omega(\cos\theta)S(\omega,\theta+\varphi) \neq P(\omega,\theta+\varphi) \qquad (6.5)$$

However, we may combine the partial derivatives to provide a function free of directional artefacts:

$$M(u,v) = |P(u,v)|^2 + |Q(u,v)|^2 = [\ \omega|S(u,v)|\ ]^2 \qquad (6.6)$$

where $M(u, v)$ is the corresponding gradient spectra. $M(u, v)$ is the mathematic non-linear combination between the surface partial derivatives $P(u, v)$ and $Q(u, v)$ in the frequency main, in which the surface directional artefact apart from those directly inherent from the surface spectrum has been removed. In the other words, the directionalities of $M(u, v)$ present the surface orientations only, which give us the ability to design the surface rotation invariant classification scheme.

We can readily see that the orientation of gradient spectra $M(u, v)$ only depends on the orientation of surface spectra $S(u,v)$ since ω is a rotation invariant scalar. Note that gradient spectra $M(u, v)$ is not equivalent to the Fourier transform of gradient space $G(p, q)$ presented in Chapter *5* where its directionality component is not removed.

From equation (6. 3), (6. 4) and (6. 6), we note that the spectra of the derivative fields $P(u,v)$ and $Q(u,v)$ have the directionality of the derivative fields. While the gradient spectra $M(u, v)$ is a combination of $P(u,v)$ and $Q(u,v)$ they do not have any directional component apart from those directly inherent from the surface spectrum $S(u,v)$. Note that

$$M(\omega,\theta+\phi)=\left[\omega\left|S(\omega,\theta+\phi)\right|\right]^2=M_\phi(\omega,\theta) \tag{6. 7}$$

hence rotation of the surface should produce a pure rotation of the corresponding *M(ω, θ)* spectrum, shown in *Figure 6. 7*.

Finally, it is interesting to note that the measures of *M(u, v)* spectrum presented in equation (6. 6) is obviously non-linear, and the following chapters no longer rely on the linearization presented in Chapter *3* and Chapter *4*.

6.3.3 Directional Characteristic of M(ω, θ)

In this section, we will test the gradient spectrum *M(ω, θ)* on both synthetic textures and real textures in terms of its ability to discriminate and determine directionality for different kinds of textures.

- ***Synthetic textures***

Firstly, we examine the gradient spectra *M(ω, θ)* of four synthetic textures, which have already been introduced and defined in chapter 3. The four textures in montage format (see *Figure 6. 6*) are *rock* (left-top), *sand*(right-top), *malv*(left-bottom) and *ogil*(right-bottom).

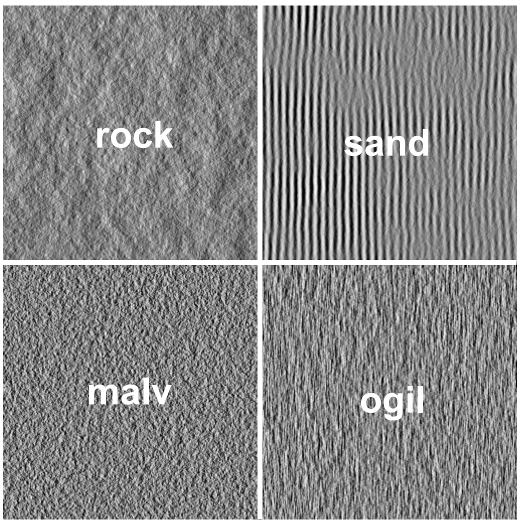

Figure 6. 6 Four synthetic textures in montage format at surface rotation $\varphi = 0°$ with constant illumination tilt angle $\tau = 0°$ and slant angle $\sigma = 50°$

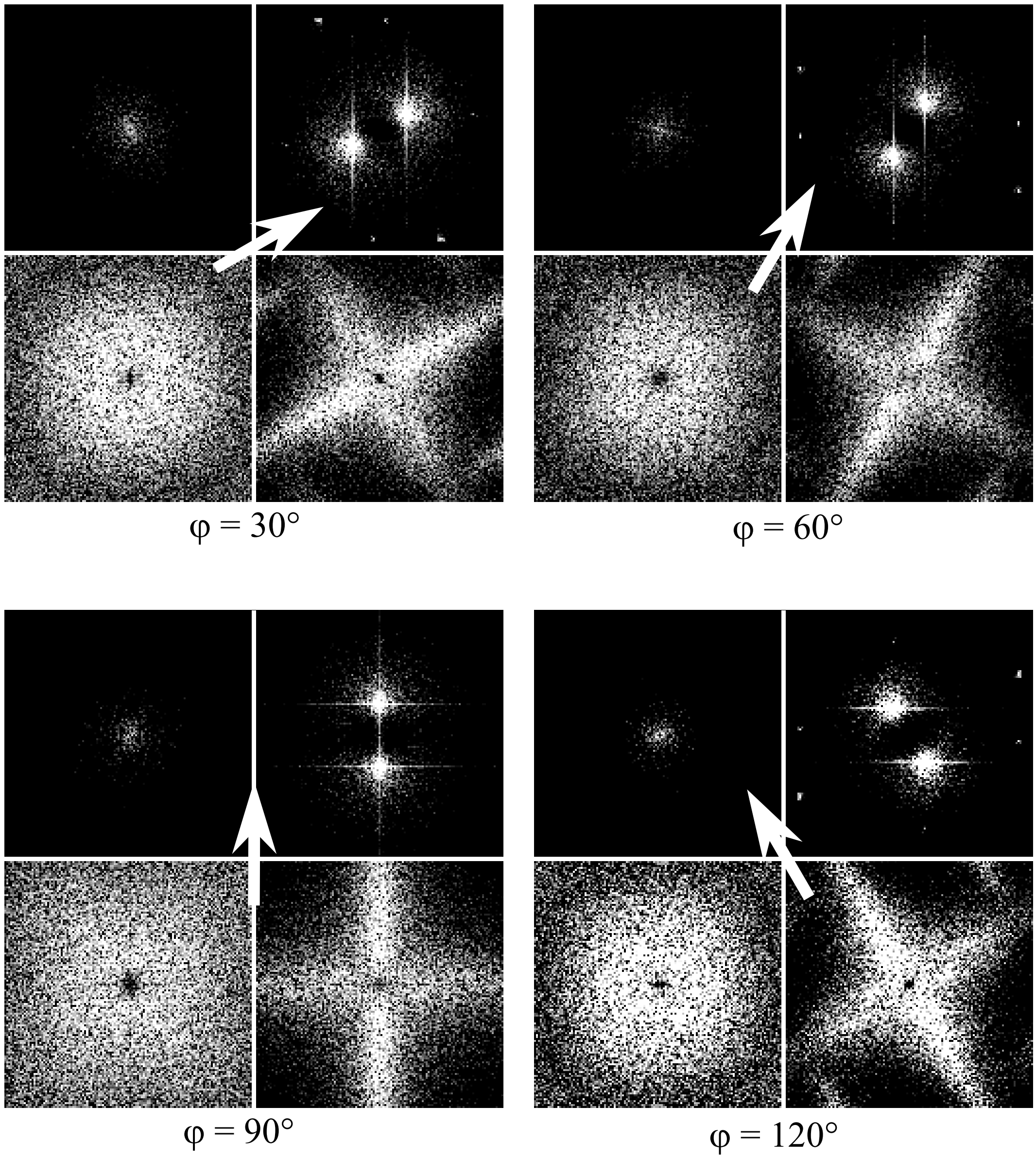

Figure 6. 7 Gradient spectra $M(\omega, \theta)$ of 4 synthetic textures shown in montage format for 4 surface rotations ($\varphi = 30°, 60°, 90°$ and $120°$). The textures are rock (left-top), sand(right-top), malv(left-bottom) and ogil(right-bottom).

From *Figure 6. 7* , which shows the $M(\omega, \theta)$ gradient spectra of four synthetic textures, it can be seen that rotation of each of the surface ($\varphi = 30°, 60°, 90°$ *and* $120°$) produces a corresponding rotation of their gradient spectra $M(\omega, \theta)$. On the other hand, the directionality in the directional (*sand*) or bi-directional (*ogil*) texture surfaces results in the directionality of the distribution of gradient spectra $M(\omega, \theta)$. This rotation variant property, $M_\varphi(\omega, \theta) = M(\omega, \theta + \varphi)$, is very important to our surface rotation invariant texture classification scheme, because the directionality of a surface is an important cue to its identification.

Also, it is very interesting to note that whether the textures are isotropic ones or directional ones, the nature or shape of distributions in the gradient spectra $M(\omega, \theta)$ is insensitive to the variation of surface rotations. We note that, theoretically, the shape of the gradient distribution will be unique and unchanged for a certain texture, although it may be rotated due to surface rotation.

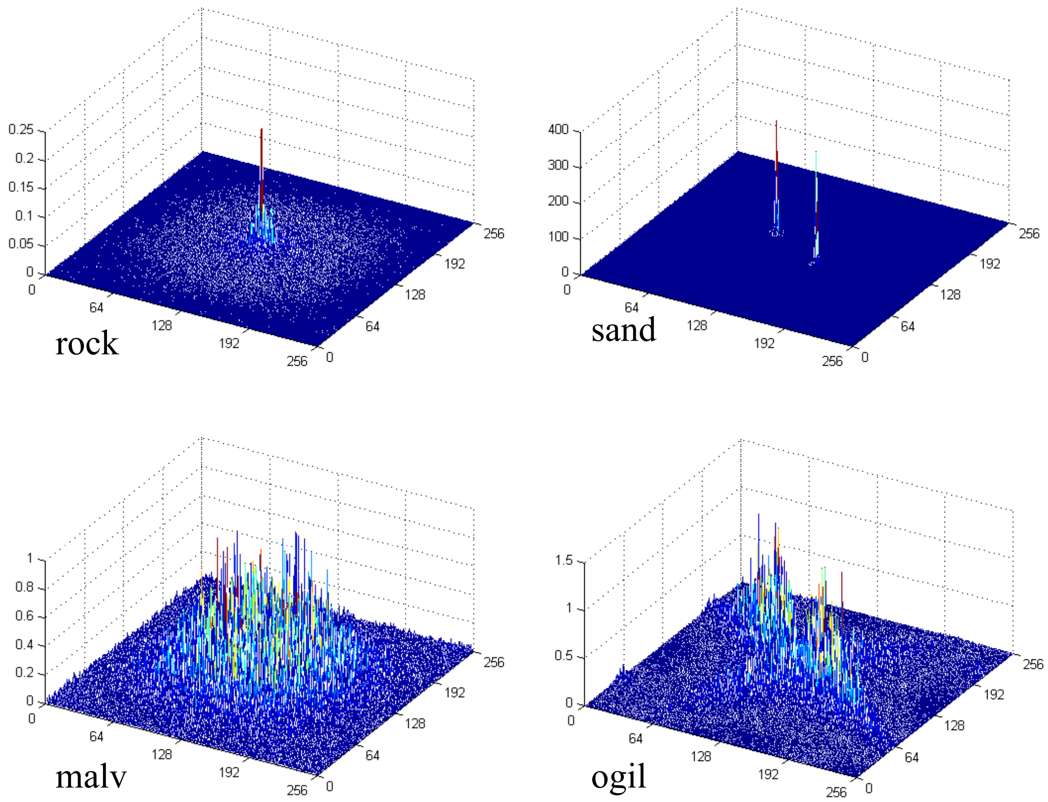

Figure 6. 8 $M(\omega, \theta)$ as a frequency distribution within a 3D gradient spectra domain for 4 synthetic textures (surface orientation $\varphi = 30°$).

By plotting gradient spectra $M(\omega, \theta)$ as a frequency distribution within a 3D gradient spectra domain, a distinctive representation of the distribution can readily be obtained as shown in *Figure 6. 8*.

We consider some of the useful information for texture description which can be interpreted from the gradient spectra $M(\omega, \theta)$:

(1) the prominent peaks in the gradient spectra give the principal direction of the texture surface;

(2) the location of the peaks gives the fundamental spatial period of the texture; and

(3) the gradient spectra are symmetric about the origin, so that only half of the frequency plane needs to be calculated.

It is the nature of the observed distributions in the gradient spectra domain that gives us very useful descriptive signatures for the observed surface textures. Considering the different textures, each texture produces a distinctive gradient spectra. For example, *rock* produces a distribution of circular pattern with an impulse in the centre, while *sand* produces two impulses linear pattern. In this case, the form and parameter of the distribution may be analysed later on and we may apply and identify these characters of distribution in gradient spectra domain and incorporate them into our surface rotation invariant texture classification scheme.

Note that in this thesis we only consider the magnitude information in gradient spectrum $M(\omega, \theta)$, while the phase information is ignored.

- ***Real textures***

Here we examine the gradient spectra $M(\omega,\theta)$ of real textures for their discrimination abilities and directionality. *Figure 6. 9* shows the gradient spectra M(ω, θ) of four real textures *(gr2, wv2, grd1, an4)* at three surface rotations $\varphi = 30°, 90°$ *and* $150°$, with the surface orientations $\varphi = 0°$. In addition, in order to show that the $M(\omega, \theta)$ functions of the rotated textures are simply a rotation of the original $(\varphi = 0°)$ $M(\omega, \theta)$ function as predicted, we plot gradient spectra $M(\omega, \theta)$ as a frequency distribution within a 3D gradient spectra domain for real textures *wv2* at surface orientations $\varphi = 0°, 30°, 60°, 90°$ (*Figure 6. 10*). This shows that the $M(\omega, \theta)$ function simply rotates by the angle of surface rotation.

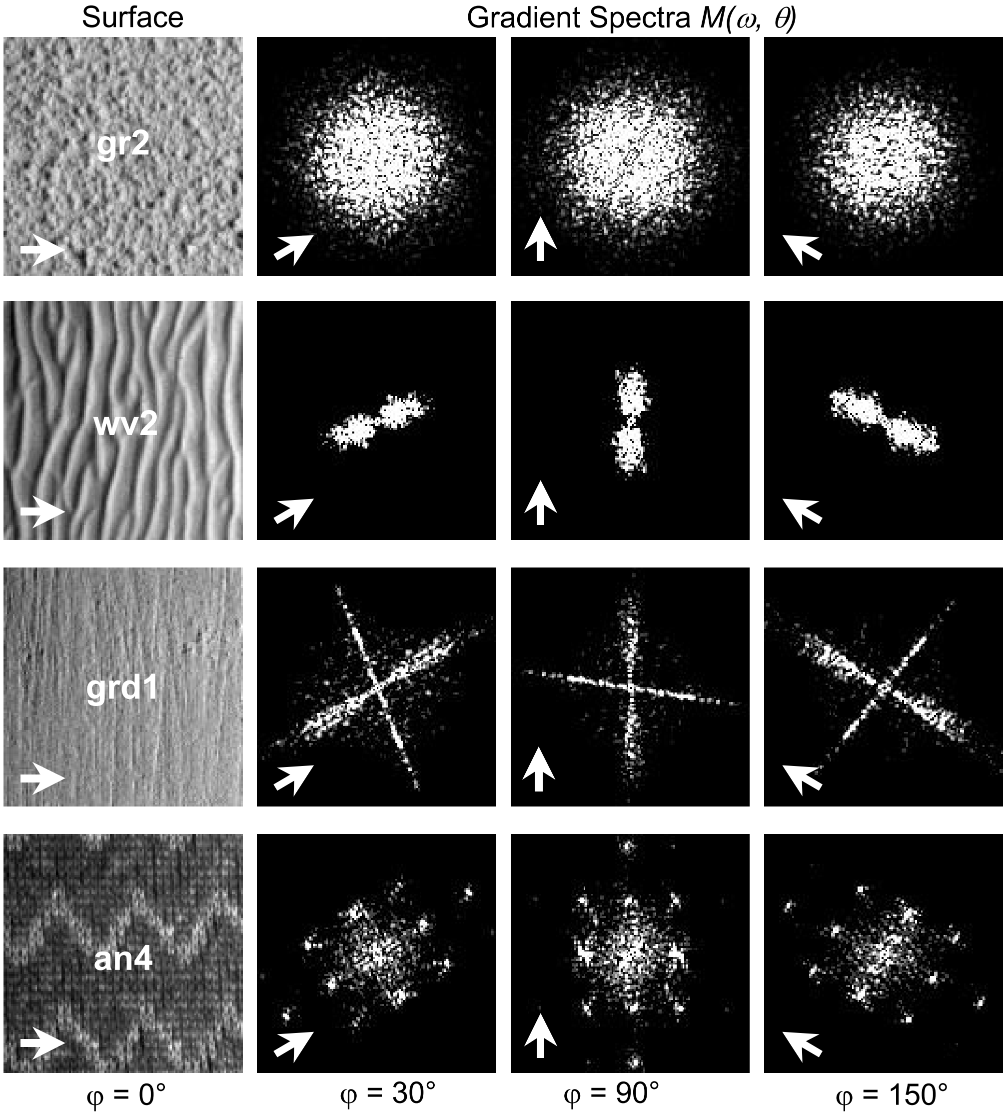

Figure 6. 9 Gradient spectra $M(\omega, \theta)$ of 4 real textures (gr2, wv2, grd1, an4) at 3 surface rotations ($\varphi = 30°$, $90°$ and $150°$). The white arrows indicate the surface corresponding orientations.

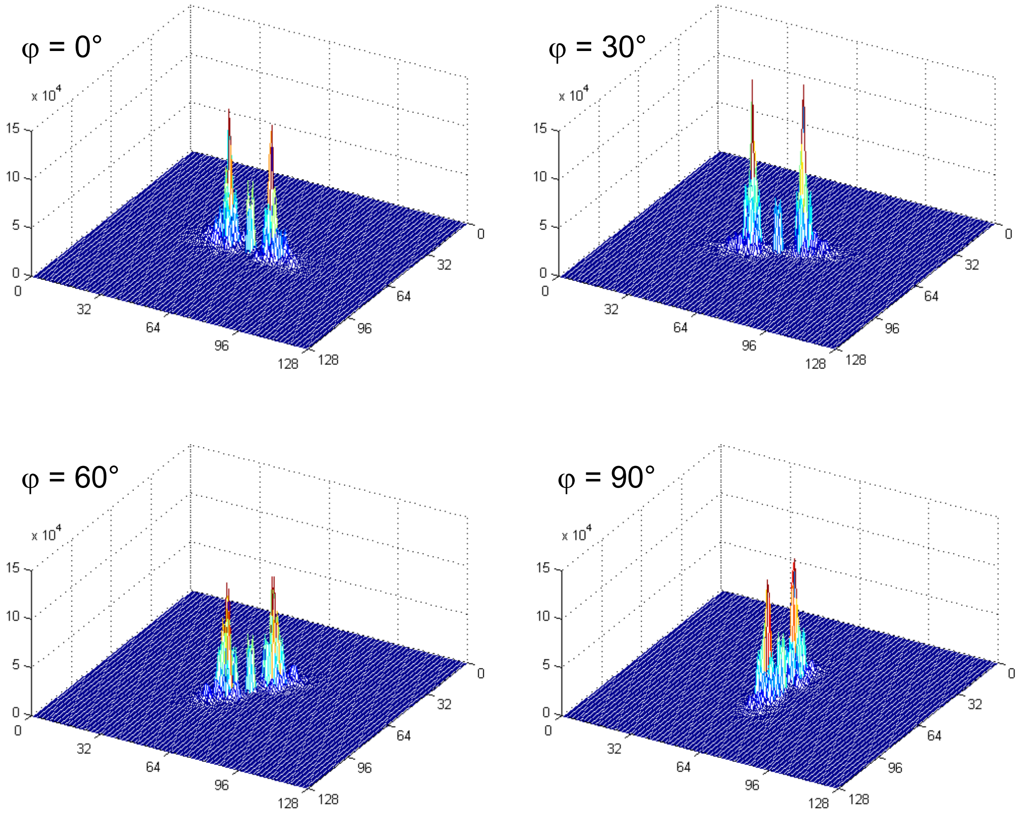

Figure 6. 10 $M(\omega, \theta)$ as a frequency distribution within a 3D gradient spectra domain for real textures wv2 at surface orientation $\varphi = 0°, 30°, 60°, 90°$.

6.3.4 Summary

In the previous sections we note that in our surface rotation invariant texture classification scheme, we will directly use surface relief characteristics rather than image intensity characteristics so that the classifier will be robust to surface rotation. Therefore the surface partial derivatives are estimated using photometric stereo. It uses multiple images of the same scene obtained under different illumination orientations. However, the surface partial derivatives are not surface rotation invariant features. Moreover they represent a two dimensional vector quantity rather than a scalar field and contain directional artefacts.

Firstly, we therefore transfer the surface partial derivatives into the frequency domain and form the gradient spectra function $M(\omega, \theta)$ which is free of directional artefacts. Secondly, we assess the discrimination ability and directionality of gradient spectra $M(\omega, \theta)$ on both synthetic textures and real textures. The results show that a rotation of the surface produces a corresponding rotation of its gradient spectrum $M(\omega, \theta)$. Also it is not surprising to note that the nature of gradient spectrum $M(\omega, \theta)$ provides very useful information relating to the type of surface structure (isotropic, directional or bi-directional) and the predominant orientation of the surface textures. Hence we may use this distinctive information in our surface rotation invariant texture classification scheme.

For classification we need to match the spectra of test and training textures in a rotation invariant manner. Comparing the gradient spectra of a test texture with those of the training classes over a complete range of rotations is computationally prohibitive. For example, for each rotated test texture sample, we have to perform *180* rotations on its gradient spectra $M(\omega, \theta)$ image in order to estimate its orientation angle between the test sample and training sample.

In the next section, we therefore use a function to compress the data but maintain their major characteristics of directionality: the *polar spectrum*. The main motivation for using polar spectrum is that we reduce the number of feature measures compared with the gradient spectrum $M(\omega, \theta)$. Polar spectrum also gives us the ability to estimate the surface orientation with less computation than those directly calculated from gradient spectra $M(\omega, \theta)$.

6.4. Polar Spectrum

6.4.1 Introduction

In this section, regarding classification we must first decide which characteristics of the texture should be measured to produce descriptive parameters. The particular resulting parameter values comprise the feature vector for each texture object. Proper selection of the features is important since only these will be used to identify the textures. Therefore, we will initially extract useful features from gradient spectra $M(\omega, \theta)$ using the polar spectrum.

The polar spectrum can be used to generate the rotation invariant features which are sensitive to texture directionality and capture the directionality of textures at different orientations. Davis [Davis81] introduces this new tool, known as a *polarogram* and uses it to achieve invariant texture features.

We have to assess the discrimination ability of the polar spectrum, in which the features should be significantly different for the textures belonging to different classes. Regarding the surface rotation, the polar spectrum should have the ability of reliability in order to enable the classifier to be robust to variance of the surface orientations and also have the ability to estimate the surface orientation angle. The advantages and drawbacks of the polar spectrum are hence considered.

Finally, we test the polar spectrum which is derived from gradient spectra $M(\omega, \theta)$ on both synthetic textures and real textures.

6.4.2 Definition of Polar Spectrum

The polar spectrum is calculated by integration of all the contributions (or values) along a line of orientation θ passing through the origin in the image of gradient spectra $M(\omega, \theta)$. We can then calculate the function of polar spectrum $\Pi(\theta)$ as:

$$\Pi(\theta) = \int_0^\infty M(\omega, \theta)\, d\omega \qquad (6.8)$$

That means the polar spectrum adds the magnitudes of all frequencies in one certain direction θ to produce a measure for the intensity in this direction. All these frequencies are lying in a radial line. The output of the polar spectrum is the variance as a function of the angle θ. This plot is used for illustrating directionality in the image. We illustrate the definition of polar spectrum in *Figure 6. 11* by demonstrating two textures (isotropic texture *gr2* and directional texture *grd1*).

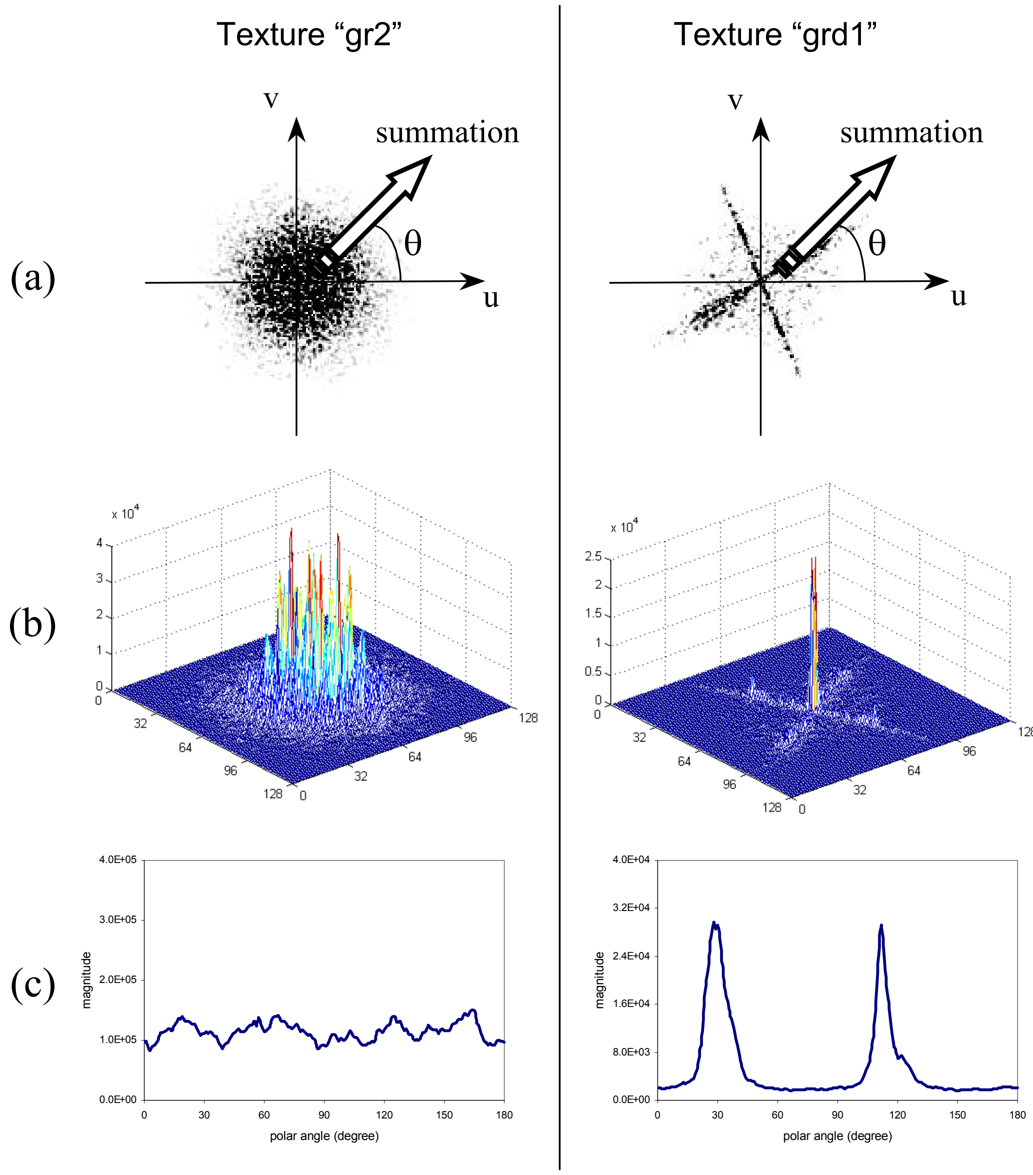

Figure 6. 11 Definition of polar spectrum Π(θ) on gradient spectra M(ω, θ) by demonstrating two textures, gr2(left column) and grd1 (right column). (a). graphical representation of polar spectrum on gradient spectra M(ω, θ); (b). M(ω, θ); (c). Polar spectra.

Note that

$$\Pi_{\phi}(\theta) = \int_{0}^{\infty} M_{\phi}(\omega, \theta) d\omega = \int_{0}^{\infty} M(\omega, \theta + \phi) d\omega = \Pi(\theta + \phi) \qquad (6.9)$$

thus a rotation of φ of a surface produces a translation of φ in the polar spectrum.

The polar spectrum $\Pi(\theta)$ is derived from the gradient spectrum $M(\omega, \theta)$ simply by expressing the spectrum in polar coordinates. It is obvious that the texture's gradient spectra are rotation dependent and it is a periodic function of θ with a period of π.

Recalling the *Figure 6. 11*, we may note that the polar spectrum of directional texture *grd1* shows prominent peaks at intervals of $90°$, which clearly correspond to the periodicity in the gradient spectra. Moreover, in the gradient spectra $M(\omega, \theta)$ of texture *grd1* is directional and so the polar spectrum $\Pi(\theta)$ tends to be a peak (at $\theta=30°$, $120°$). On the other hand, there are no peaks or marked directionality in the polar spectrum of isotropic texture *gr2*. This observation indicates the usefulness of the polar spectrum $\Pi(\theta)$ in summarising the directional properties of a texture.

6.4.3 Drawbacks and Solutions

Prior to discussing the properties of the polar spectrum in terms of directionality and the effects of surface rotation, we have to consider some of its drawbacks.

- **Interpolation**

The gradient spectra are calculated by using a discrete FFT. Hence the polar spectrum $\Pi(\theta)$ (equation *(6. 8)*) is obtained by summing discrete coefficient values:

$$\Pi(\theta) = \sum_{\omega=1}^{R} M(\omega, \theta) \qquad (6.10)$$

where R is the radius high frequency range of a circle centred at the origin. For an $N \times N$ gradient spectra $M(\omega, \theta)$, R is typically chosen as $N/2$.

Therefore, while calculating the value of $\Pi(\theta)$, noises will be introduced since the gradient data is produced in a Cartesian described from $M(\omega, \theta)$ and has a finite resolution. In *Figure 6. 12(a)*, we note that some of the points on the calculating line of *R2* at the polar angle θ do not correspond to any points of the $M(\omega, \theta)$ spectra, compared to those points along the line of *R1*. An interpolation algorithm was implemented in order to estimate the new point values on the line of *R2*. Depending on the amount of detail present in the spectrum along with the final requirements of the images, an appropriate interpolation scheme may be employed. In our circumstance, since a pixel falling between locations will always be somewhere in between four valid pixel locations, four pixels (*pt.1, pt.2, pt.3 and pt.4*) surrounding the calculated pixel location (*desired pt.*) will be used to contribute to the estimation of the desired coefficient, shown in *Figure 6. 12 (b)*.

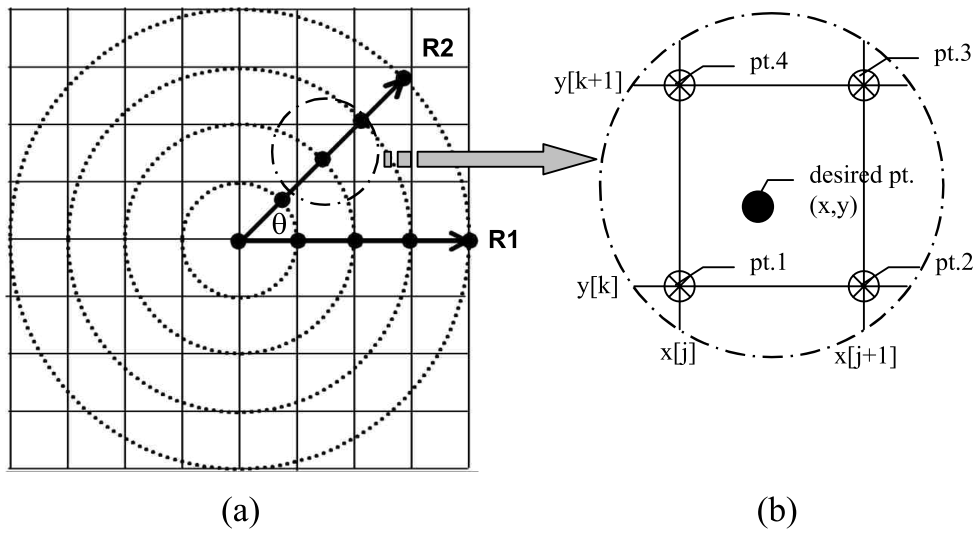

Figure 6. 12 Illustrating effect of interpolation while calculating polar spectrum $\Pi(\theta)$ from discrete Cartesian M(u,v) spectra. (a). Effect on a grid square. (b). Definition of the grid square.

The simplest interpolation is *bilinear* interpolation in the grid square [Press92]. The aim of this interpolation is to estimate the function *f(x,y)* at some untabulated point (x_i, y_i). This can be performed using the values of the function at the four tabulated points that surround the desired interior point. This is illustrated in *Figure 6. 12(b)*. This figure defines j and k as:

$$
\begin{aligned}
x[j] \leq x_i \leq x[j+1] \\
y[k] \leq y_i \leq y[k+1]
\end{aligned}
\qquad (6.11)
$$

and then

$$
\begin{aligned}
f_1 &= \mathrm{f}\,(\,x[j], y[k]\,) \\
f_2 &= \mathrm{f}\,(\,x[j+1], y[k]\,) \\
f_3 &= \mathrm{f}\,(\,x[j+1], y[k+1]\,) \\
f_4 &= \mathrm{f}\,(\,x[j], y[k+1]\,)
\end{aligned}
\tag{6. 12}
$$

The formulae of the interpolation is then given by :

$$
\begin{aligned}
t &\equiv \frac{x_i - x[j]}{x[j+1] - x[j]} \\
u &\equiv \frac{y_i - y[k]}{y[k+1] - y[k]}
\end{aligned}
\tag{6. 13}
$$

$$
y(x_i, y_i) = f_1 \times (1-t) \times (1-u) + f_2 \times t \times (1-u) + f_3 \times (1-u) \times t + f_4 \times t \times u \tag{6. 14}
$$

- **Frequency range selection : low frequency f_{low}**

One of the problems with the interpolation algorithm is that the estimated point values near the centre frequency ($\omega=1$) provide poor angular resolution. Therefore, we modify the definition of polar spectrum $\Pi(\theta)$ in equation *(6. 10)* to a band-pass filter:

$$
\Pi\ (\theta) = \sum_{\omega=f_{low}}^{f_{high}} M(\omega,\theta) \tag{6. 15}
$$

where f_{low} and f_{high} are used in the band-pass filter, which is illustrated in *Figure 6. 13*.

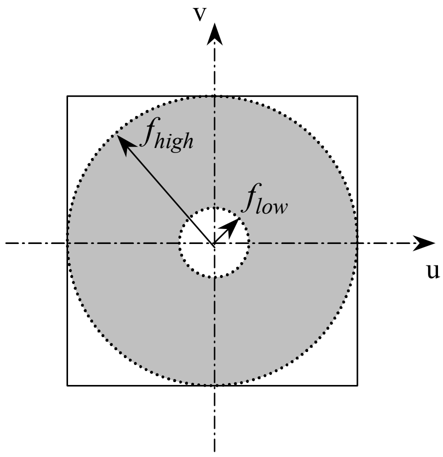

Figure 6. 13 Frequency range selection of band-pass filter while calculating polar spectrum.

This effect can readily been seen in *Figure 6. 14*, which plots the polar spectrums of texture "*grd1*" derived from calculations in different low frequency ranges $(\omega = 1,\ \omega = 2,\ and\ \omega = 8)$. For the size of $N \times N$ gradient spectra $M(\omega, \theta)$, f_{high} is set to $N/2$ as default, while we change the f_{low} to the value of *1*, *2* and *8* respectively. It is clear to see that the peaks of *A1* and *A2* in the polar spectrum with $f_{low} = 1$ are the correct ones derived from the dominant directionalities in gradient spectra $M(\omega, \theta)$. However, the peaks of *B1* and *B2* come from the interpolation noise at certain polar angles θ of about 45° and 135° respectively and do not correspond to the directionality in the gradient spectra $M(\omega, \theta)$. On the other hand, increasing the low frequency range f_{low} to the value of *8*, the noise disappears due to the increased angular resolution at this frequency.

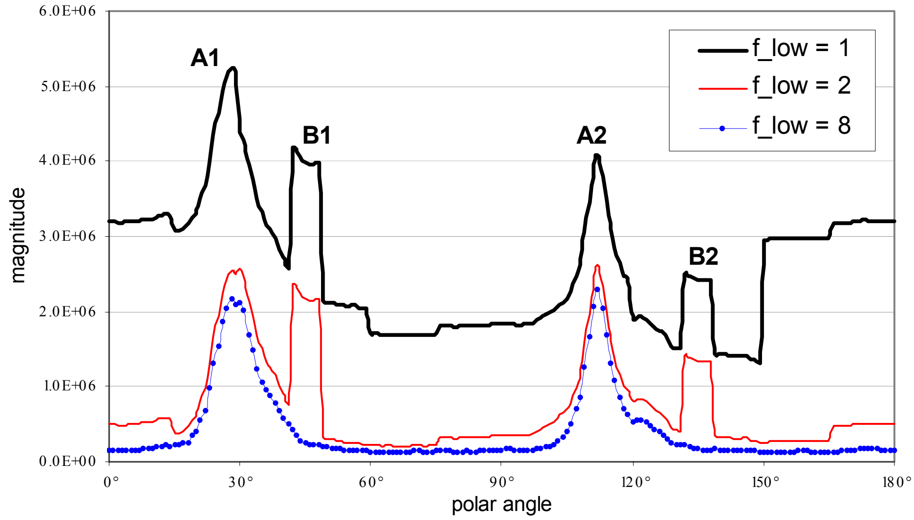

Figure 6. 14 Polar spectrums of texture "grd1" derived from calculating in different low frequency ranges ($\omega = 1$, $\omega = 2$, and $\omega = 8$).

It is worth noticing that increasing the low frequency range results in decreasing the polar spectra magnitude or energy. This is illustrated in *Figure 6. 15*.

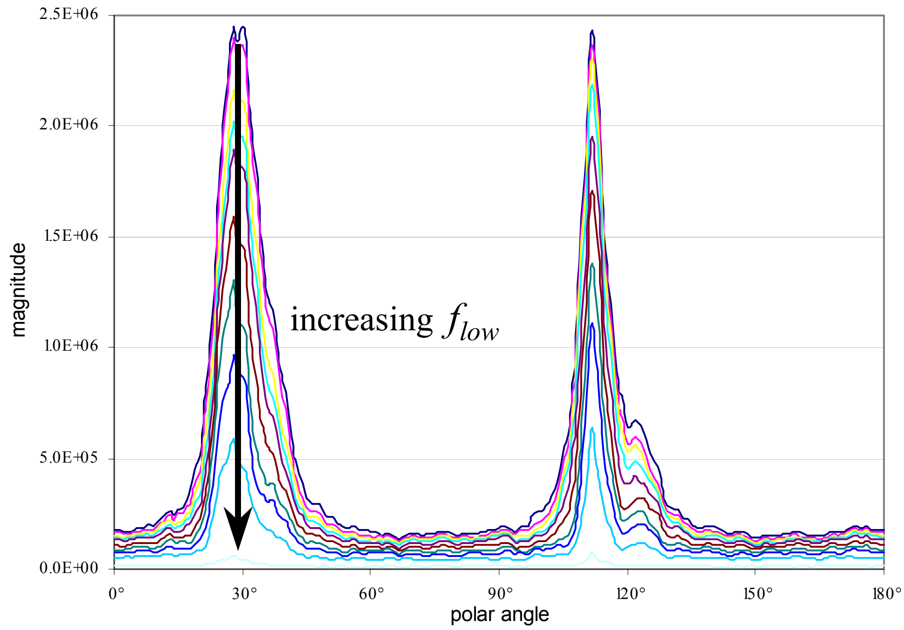

Figure 6. 15 Increasing the low frequency range results in decreasing the polar spectra magnitude or energy as more and more components of M(u, v) are neglected (low frequency value f_{low} starts from 4 to 64) for texture grd1.

In general, the estimated point values near the centre frequency (ω=*1*) provide poor angular resolution (*Figure 6. 14*). On the other hand, increasing the low frequency range results in decreasing the polar spectra magnitude (*Figure 6. 15*). We decide to set the low frequency range starting at the value of 8.

- **Frequency range selection : high frequency f_{high}**

Regarding equation *(6. 15)*, the band-pass filter is applied to the gradient spectra. In this case we will also lose some of the information in high frequency range. However, most of the image power is concentrated in the low frequency components. This is highlighted by circles superimposed at different radii on the gradient spectra. We calculate the proportion of the total sum of gradient spectra $M(\omega, \theta)$ over the entire domain contained within each circle, then we find the relationship shown in the *Table 6. 1* (f_{low}= *1*). We note that with the high frequency f_{high} set to *64*, the image width of gradient spectra will be *128* and we still have most of the power *(99.35%)* of the image. Therefore, we will set gradient spectra size to 128×128 pixels as the default setting in further investigations, since it will give us enough information for the post-processing.

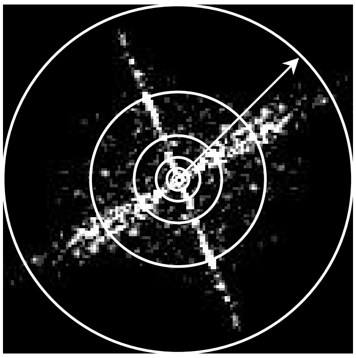

$2 \times f_{high}$ (cycles/image-width)	% image power
2	71.80%
4	81.95%
8	84.71%
16	89.92%
32	96.33%
64	99.35%
128	99.98%

Table 6. 1 The percentage of gradient spectra power $M(\omega, \theta)$ with increasing high frequency f_{high} for texture grd1 (f_{low}= 1).

6.4.4 Polar Spectrum is a Function of Texture Directionality

In this section, we will test the polar spectrum as a function of texture directionality using four synthetic textures and four real textures.

- ***Synthetic textures***

Polar spectra of the four selective synthetic textures *(rock, sand, ogil and malv)* defined in chapter 3 on gradient spectra $M(\omega, \theta)$ at surface rotation of $\varphi = 30°$ are shown in *Figure 6. 16*. It is interesting to note that there are no marked peaks on the polar spectrum for isotropic texture *rock* and *malv*, while there is a sharp peak *A* at the polar angle $\theta = 30°$ on the polar spectrum of the directional texture *sand*. There are two peaks, *B1* at the polar angle $\theta = 30°$ and *B2* at the polar angle $\theta = 120°$, on the polar spectrum of the bi-directional texture *ogil*, although *B2* is not the dominant direction having viewed the original surface. In general, all of the peaks appearing on the polar spectrum do correspond to the directionality of the original textures.

- ***Real textures***

We repeat this process on four selective real textures *(gr2, wv2, grd1* and *an4)*. The results are shown below in *Figure 6. 17*. The same conclusions can also be made: the polar spectrum is a function of texture directionality. It is obvious that for a given texture surface, the texture directionality varies with change of orientation. These changes in directionality can be captured by the polar spectrum. For example, the directionality of texture *wv2* can be characterised by peak *A*, on the other hand, the directionalities of texture *an4* may be presented as peaks *D*, *E* and *F* in its corresponding polar spectrum $\Pi(\theta)$.

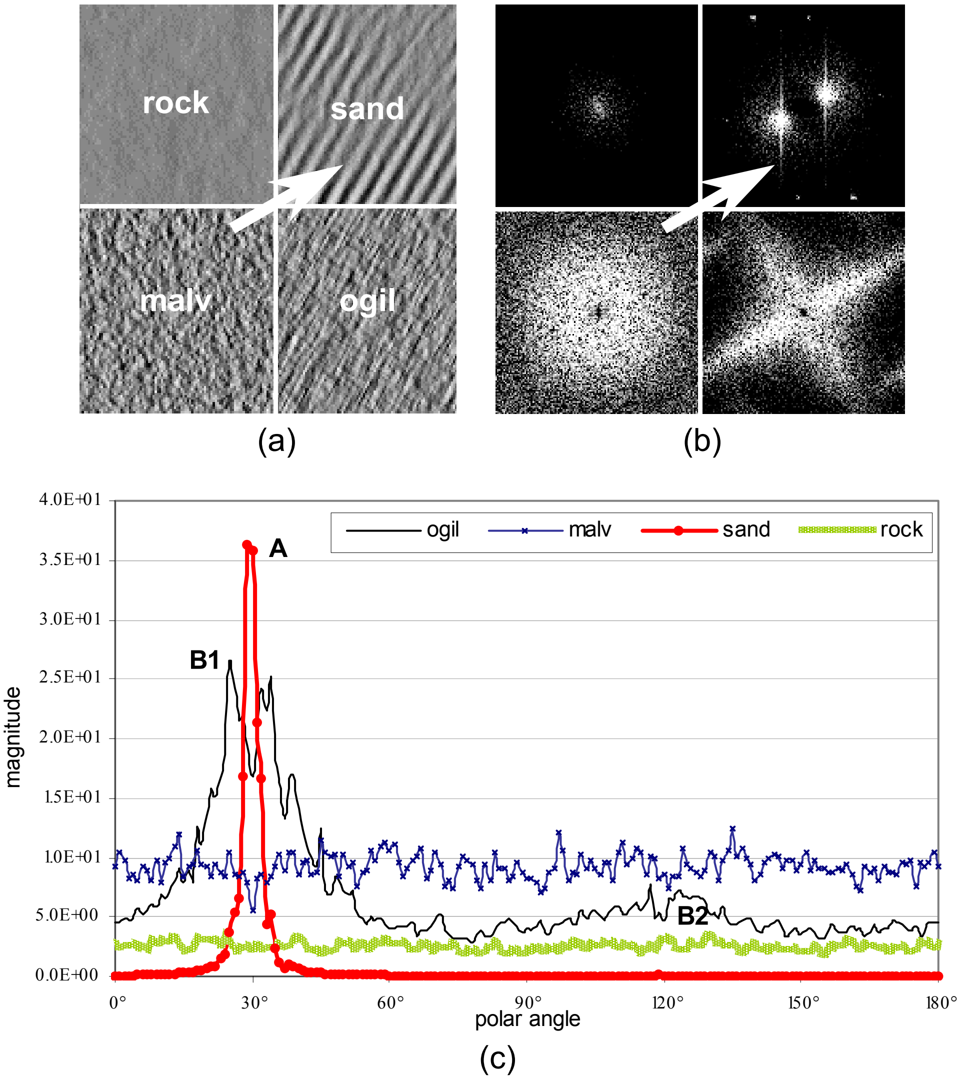

Figure 6. 16 Polar spectrums of four selective synthetic textures (rock, sand, ogil and malv) on gradient spectra $M(\omega, \theta)$ at surface rotation of $\varphi = 30°$. (a). surface at constant tilt angle $\tau = 0°$; (b) gradient spectra; (c) polar spectrum.

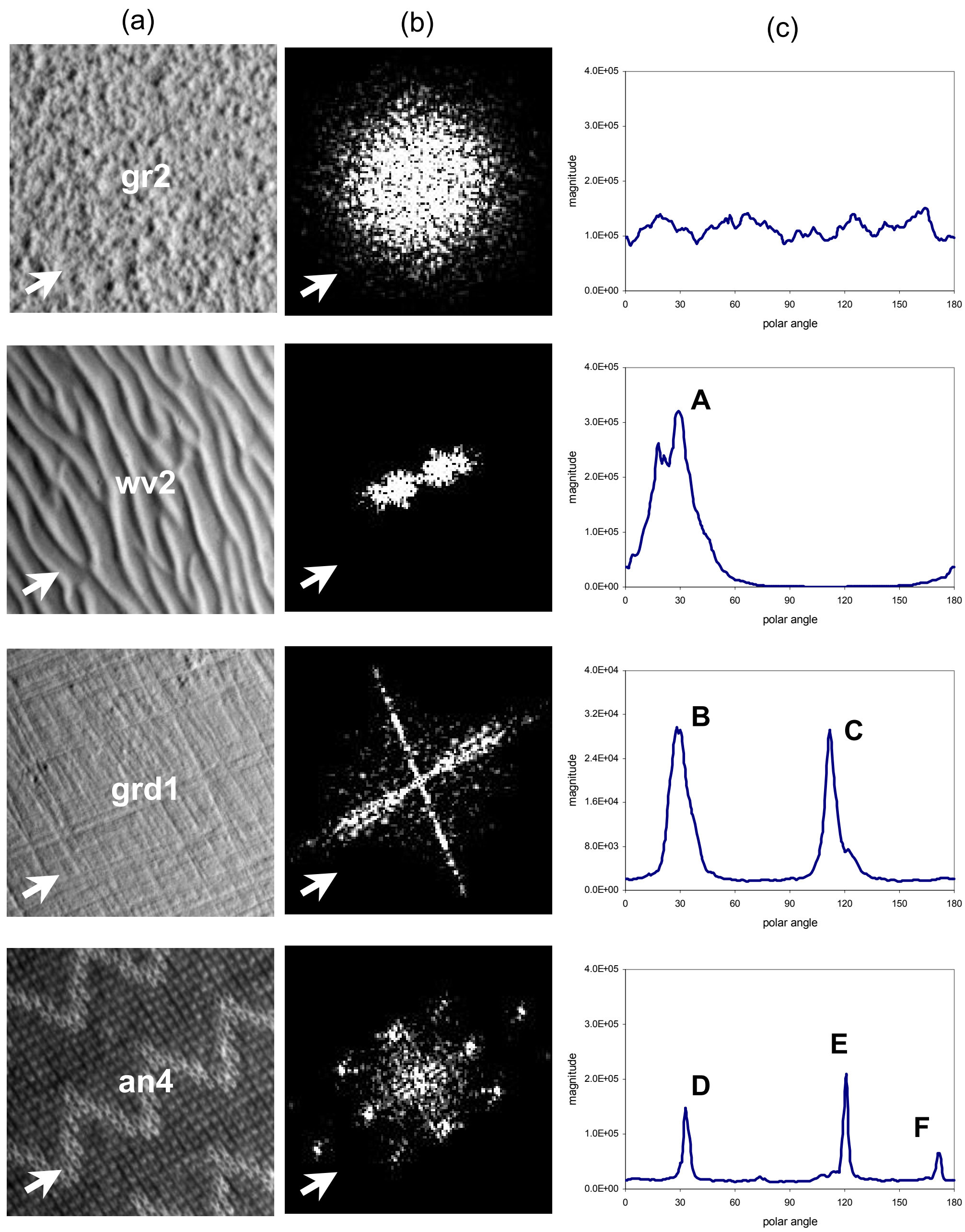

Figure 6. 17 Polar spectrums of four selective real textures (gr2, wv2, grd1 and an4) on gradient spectra $M(\omega, \theta)$ at a surface rotation of $\varphi = 30°$. (a). surface at constant tilt angle $\tau = 0°$; (b) gradient spectra; (c) polar spectrum.

6.4.5 Polar Spectrum at Different Surface Orientations

Note that while both gradient spectra $M(\omega,\theta)$ and its polar spectrum do not theoretically contain any directional artefacts such as a directional filtering effect, they are, rotationally sensitive. That is, if the surface is rotated by an angle φ then a new gradient spectra $M_\varphi(\omega, \theta)$ and a new polar spectrum $\Pi_\varphi(\theta)$ will result (see *Figure 6. 18*), such that in theory:

$$\Pi_\varphi(\theta) = \Pi(\theta + \varphi) \qquad (6.16)$$

This implies that a rotated texture's polar spectrum $\Pi_\varphi(\theta)$ is equivalent to a translation of its polar spectrum $\Pi(\theta)$ by the same amount φ along the orientation axis. For comparison images taken under surface rotation are shown individually and all captured images are at a constant illuminant tilt angle $\tau = 0°$ (90° and 180° illuminant tilt angle images are also captured for the photometric stereo process but are not shown here). Comparison of the images at $\varphi = 0°$ and $\varphi = 90°$ shows that they are not simple rotations of each other. In the image corresponding to $\varphi = 0°$ the vertical lines of the texture are clearly presented. While in the image corresponding to $\varphi = 90°$ the texture has been attenuated and the lines which should be horizontal are no longer visible.

On the other hand, this is not surprising. *Figure 6. 19* illustrates the relationship between $\Pi_\varphi(\theta)$ and $\Pi(\theta + \varphi)$. By depicting the polar spectrums of the rotated *"wv2"* surface, this shows that a rotated texture's polar spectrum is an approximate translation of the unrotated texture's polar spectrum, and that the degree of each translation approximates to the corresponding rotation of the surface.

6.4.6 Estimation of Surface Orientation via Polar Spectrum

Obviously since the polar spectrum is rotationally sensitive, we cannot directly use polar spectra for surface rotation invariant classification. We have to estimate the surface orientation angle first for each test texture and then compare the test texture's polar spectrum to the training textures' polar spectra. This is done by translating each by the estimated surface orientation angle.

In the section, we will estimate the surface orientation angle of the polar spectrum by using the simple sum of squared difference metric. The estimation process will be presented in the next section. We also discuss surface orientation estimation obtained from gradient spectra and gradient space.

- ***Estimation of surface orientation***

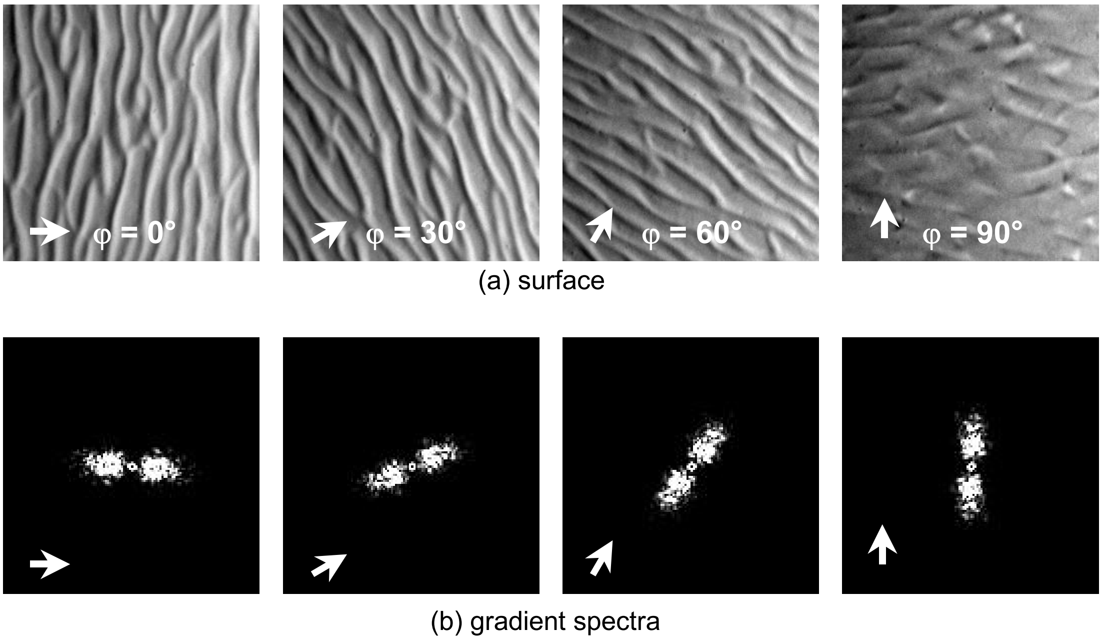

Figure 6. 18 Textures "wv2" on gradient spectra $M(\omega, \theta)$ at different surface rotations of φ = 0°, 30°, 60° and 90° (the white arrows indicate the surface orientations). (a) surface at constant tilt angle τ = 0°; (b) gradient spectra.

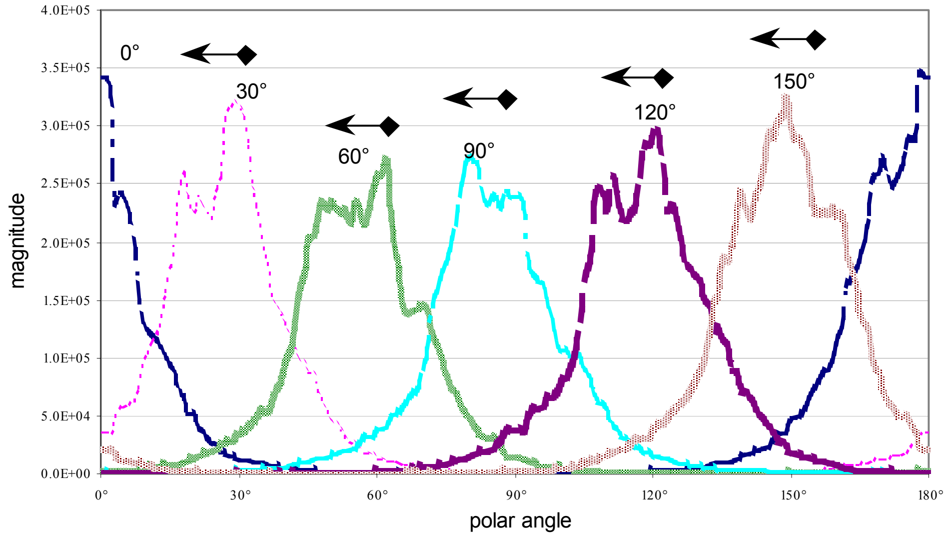

Figure 6. 19 Polar spectrums of real textures "wv2" at surface rotations of φ = 0°, 30°, 60°, 90°, 120° and 150°.

Figure 6. 19 shows polar spectra of real textures *"wv2"* at surface rotations of φ = *0°, 30°, 60°, 90°, 120°* and *150°*, some examples of corresponding gradient spectra $M(\omega, \theta)$ are shown in *Figure 6. 18.* As the polar spectrum provides a measurement of texture directionality. It can be used to estimate its orientation. From *Figure 6. 19*, we note that a rotated texture's polar spectrum is approximately a translation of the non-rotated texture's polar spectrum. Thus we must compare polar spectrums over a range of angular displacements (φ_{test} = 0°, 1°, 2°, ….180°) in order to determine the degree of correspondence and the relative angle of two surfaces. We use the sum of squared difference metric function *SSD* to measure the distance between two polar spectrums:

$$SSD(\varphi_{test}) = \min\left\{ \sum_{\theta=0°}^{180°} [\,\Pi_{rotated}(\theta + \varphi_{test}) - \Pi_{unrotated}(\theta)\,]^2 \right\} \qquad (6.17)$$

where φ_{test} = 0°, 1°, 2°, ….180°. When the cost function of $SSD(\varphi_{test})$ is minimised the angular displacement φ_{test} in the polar spectrum will be the relative angle of these two surfaces.

- ***Estimation results from directional and isotropic textures***

Table 6. 2 shows the estimated angles of surface orientation for real and directional texture "*wv2*" obtained from polar spectra. Four sample images are constructed from the images of the textures rotated individually in *Table 6. 2 (a).* We note that the results of estimated angles in *Table 6. 2 (b)* shows good performance for this directional texture "*wv2*", while the maximum error in the angle is *2°*.

On the other hand, *Table 6. 3* gives the estimated angles of surface orientation for the real isotropic texture "*gr2*" obtained from polar spectra. We can see that the estimation that took place with the surface orientation angle $\varphi = 90°$ has failed, and the error in the angle increased to *82°*.

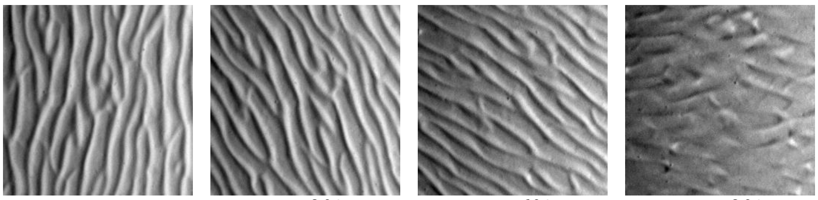

φ = 0° φ = 30° φ = 60° φ = 90°

(a)

Original surface rotation angles φ	30°	60°	90°	120°	150°	180°
Estimated angles obtained from polar spectrums	30°	60°	90°	122°	152°	179°
Error	***0°***	***0°***	***0°***	***+2°***	***+2°***	***-1°***

(b)

Table 6. 2 The estimated angles of surface orientation for the real directional texture "wv2" obtained from polar spectra. (a) some rotated surface samples at orientation angle of $\varphi = 0°, 30°, 60°$ and $90°$, while the tilt angle τ is kept constant at $0°$; (b) estimation error.

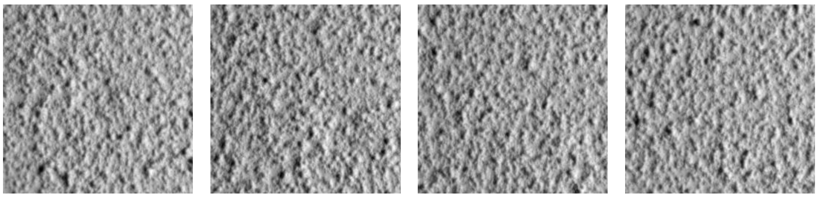

φ = 0° φ = 30° φ = 60° φ = 90°

(a)

Original surface rotation angles φ	30°	60°	90°	120°	150°	180°
Estimated angles obtained from polar spectrum	30°	60°	8°	121°	151°	181°
Error	***0°***	***0°***	***-82°***	***+1°***	***+1°***	***+1°***

(b)

Table 6. 3 The estimated angles of surface orientation for the real isotropic texture "gr2" obtained from polar spectra. (a) some rotated surface samples at orientation angle of $\varphi = 0°$, $30°$, $60°$ and $90°$, while the tilt angle τ is kept constant at $0°$; (b) estimation error.

Regarding the isotropic texture, it would be difficult to achieve better accuracy than the directional texture, because there are no obvious peaks within the polar spectrum. In this case, translating the polar spectrum $\Pi(\theta)$ may not give the correct estimation. This means that we cannot estimate the direction of an isotropic texture from the polar spectrum $\Pi(\theta)$.

- ***Comparison with those estimated from gradient spectra and gradient space***

Figure 6. 20 shows the estimates of the surface orientation angle for four synthetic textures (*rock, sand, ogil and malv*) obtained from polar spectrum $\Pi(\theta)$, gradient spectra $M(\omega, \theta)$ and gradient space $G(x, y)$. Regarding the four different textures, the estimated orientation angle obtained by the polar spectrum $\Pi(\theta)$ has the highest accuracy. In this case, most of the error angles are under $2°$ apart from one at an angle of $8°$. Those obtained by the gradient space $G(x, y)$ have the worst estimation results. While the resulting estimation angle obtained by the 2D gradient spectra $M(\omega, \theta)$ can be thought of as reasonable.

Comparing results for the different textures, the performance of the estimation on the isotropic ones (*rock* and *malv*) is worse than that for the directional ones. We also note that the estimation processing failed for the isotropic texture *rock* and *malv* in the gradient space *G(x, y)*. This is because the distribution of the gradient space for those textures does not relate well to the surface orientation and leads to the failure of the surface rotation at an angle of about *0°*. As previously mentioned, our estimation results based on the frequency domain methods (gradient spectra and polar spectrum) are much better than those obtained with the spatial domain method (gradient space).

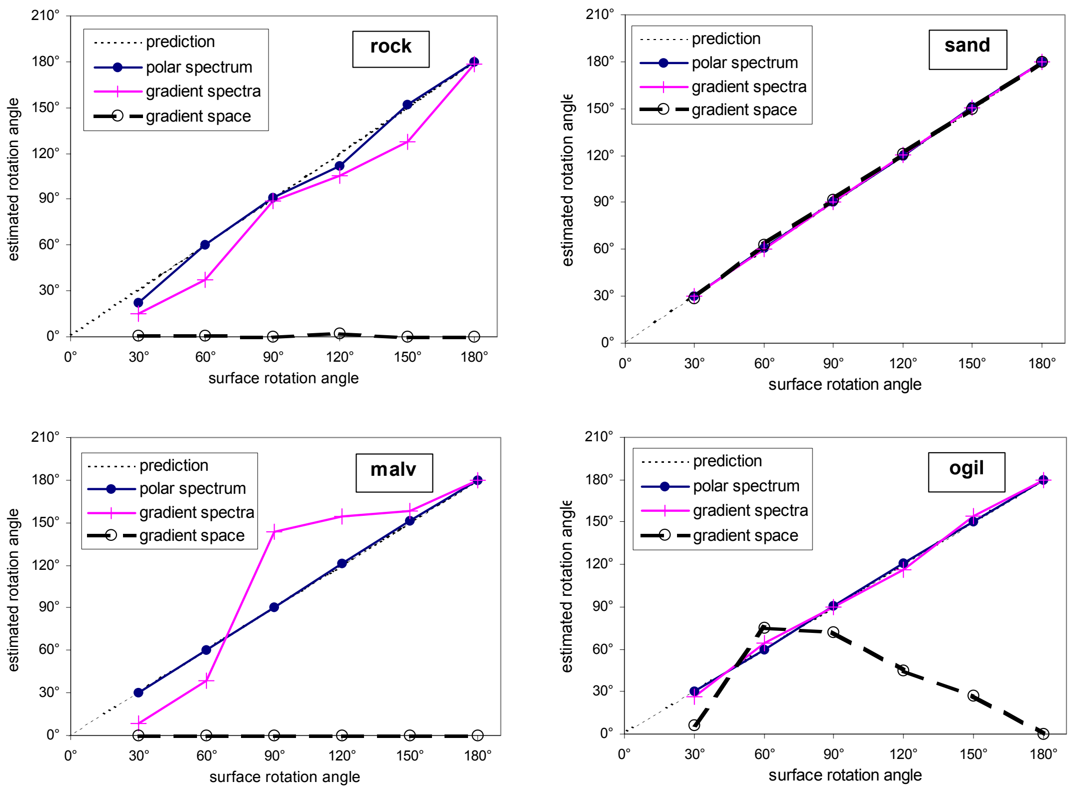

Figure 6. 20 Comparing the estimations of the surface orientation angle for four synthetic textures (rock, sand, ogil and malv) obtained from polar spectrum $\Pi(\theta)$, gradient spectra $M(\omega, \theta)$ and gradient space $G(x, y)$.

6.4.7 Summary

In the section, the polar spectrum technique was introduced. It enables us to reduce the dimension of feature space from 2D gradient spectra $M(\omega, \theta)$ to a 1D polar spectrum $\Pi(\theta)$, while maintaining the majority of useful characteristics. In addition, it also avoids the heavy computation resulting from comparing the gradient spectra $M(\omega, \theta)$ of a test texture with those of the training textures over a complete range of rotations.

Noises due to the discrete Cartesian nature of $M(\omega, \theta)$ were investigated and reduced using interpolation and a low frequency integration limit. Next, two of the main properties of the polar spectrum were investigated:

- the polar spectrum as a function of texture directionality, and
- the polar spectrum as a function of surface orientation.

Regarding these two important aspects, we confirm that a rotated texture's polar spectrum is an approximate translation of the non-rotated texture's polar spectrum and that the degree of each translation approximates to the corresponding rotation of the surface. This property of the polar spectrum allows us to estimate the surface orientation or rotation angle by comparing the polar spectrums over a range of angular displacements using the sum of the squared difference function. Finally, we discuss a comparative study on the estimation of surface orientation angles obtained from polar spectra $\Pi(\theta)$, gradient spectra $M(\omega, \theta)$ and gradient space $G(x, y)$. The results of estimation based on the polar spectrum $\Pi(\theta)$ gives the best accuracy.

In the next section, we will develop classifier using features obtained from the polar spectrum and illustrate how it works.

6.5. Classifier

In this section we will illustrate how the classifier works based on the goodness-of-fit measurement and also consider the corresponding estimated surface orientation obtained by this method.

In *Figure 6. 21*, we illustrate the goodness-of-fit measurement of the test texture's polar spectrum (*wv2* at $\varphi = 60°$) and compare it to four training textures' polar spectra obtained at the surface orientation angle $\varphi = 0°$. Consequently, the sum of squared difference (SSD) metric between the test texture *wv2* ($\varphi = 60°$) and four training textures ($\varphi = 0°$), and their corresponding estimated surface orientation angles are listed in *Table 6. 4*. We note that the minimal value of SSD *(1.14e+11)* is only achieved between the polar spectrum of the test texture *wv2* and its training polar spectrum. Moreover the estimated surface orientation angle φ_{test} *(60°)* is exactly equal to the angular displacement between the test polar spectrum and the training one for texture *wv2*. While on the other hand, the estimated surface orientation angle φ_{test} between the test texture *wv2* and the other two directional training texture (*an4* and *grd1*) is also found to be *57°* and *55°* respectively. This is because all of them have a peak of distribution at a polar angle of approximately *0°*. This illustrates that SSD evaluation can be effective.

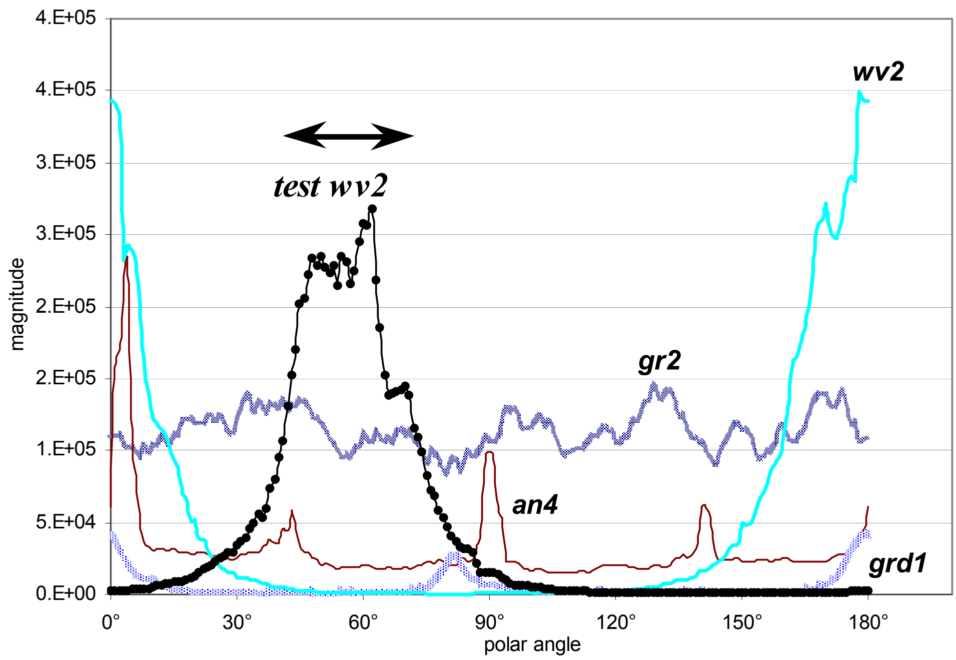

Figure 6. 21 Goodness-of-fit measurement for testing a texture's polar spectrum (wv2 at $\varphi = 60°$) against four training textures' polar spectra obtained at the surface orientation angle $\varphi = 0°$

Training textures (φ=0°)		*an4*	*gr2*	*grd1*	*wv2*
Testing texture wv2 (φ=60°)	SSD	*8.17e+11*	*1.74e+12*	*1.15e+12*	*1.14e+11*
	Estimated angle φ_{test}	*57°*	*23°*	*55°*	*60°*

Table 6. 4 Sum of squared difference (SSD) values between the test texture wv2 (φ = 60°) and four training textures (φ = 0°), together with their corresponding estimated surface orientation angles.

6.6. Summary of the Complete Algorithm

6.6.1 Surface Rotation Invariant Classification Scheme Using Photometric Stereo (Surface Information)

Now it is time to illustrate the complete surface rotation invariant classification scheme in *Figure 6. 22*. The process is as follows:

1. A photometric image set of the texture to be classified is captured by a digital camera which is fixed above the 3D rotated surface texture sample (i.e. three images are taken at illuminant tilt angles of *0°*, *90°* and *180°* respectively).
2. The photometric stereo algorithm uses this image set to estimate the surface partial derivatives $p(x,y)$ and $q(x,y)$. This enables us to use surface relief characteristics rather than the image intensity characteristics so that the classifier is to be robust to surface rotation.
3. However, the surface partial derivative $p(x,y)$ and $q(x,y)$ are not surface rotation invariant features and they are vectors containing directional artifacts as well. Therefore, they are Fourier transformed into $P(\omega, \theta)$ and $Q(\omega, \theta)$, and combined to provide the corresponding gradient spectra $M(\omega, \theta)$ which are free of directional artifacts.
4. Gradient spectra $M(\omega, \theta)$ are processed to provide polar spectra $\Pi(\theta)$. This compresses the data from 2D to 1D while maintaining the major directional characteristics. It also avoids the heavy computations involved in comparing the gradient spectra $M(\omega, \theta)$ of a test texture with those of the training texture over a

complete range of rotations.

5. The polar spectrum is compared with the polar spectra obtained from training images over a range of angular displacements (φ_{test}) using a sum of squared differences metric. The comparison results in the corresponding surface orientation angle since a rotated texture's polar spectrum is an approximate translation of the non-rotated texture's polar spectrum.
6. The total sum of squared difference metric calculated from step *5* and the best combination provides a classification decision based on the goodness-of-fit measurement and an estimate of the relative orientation of the test texture.

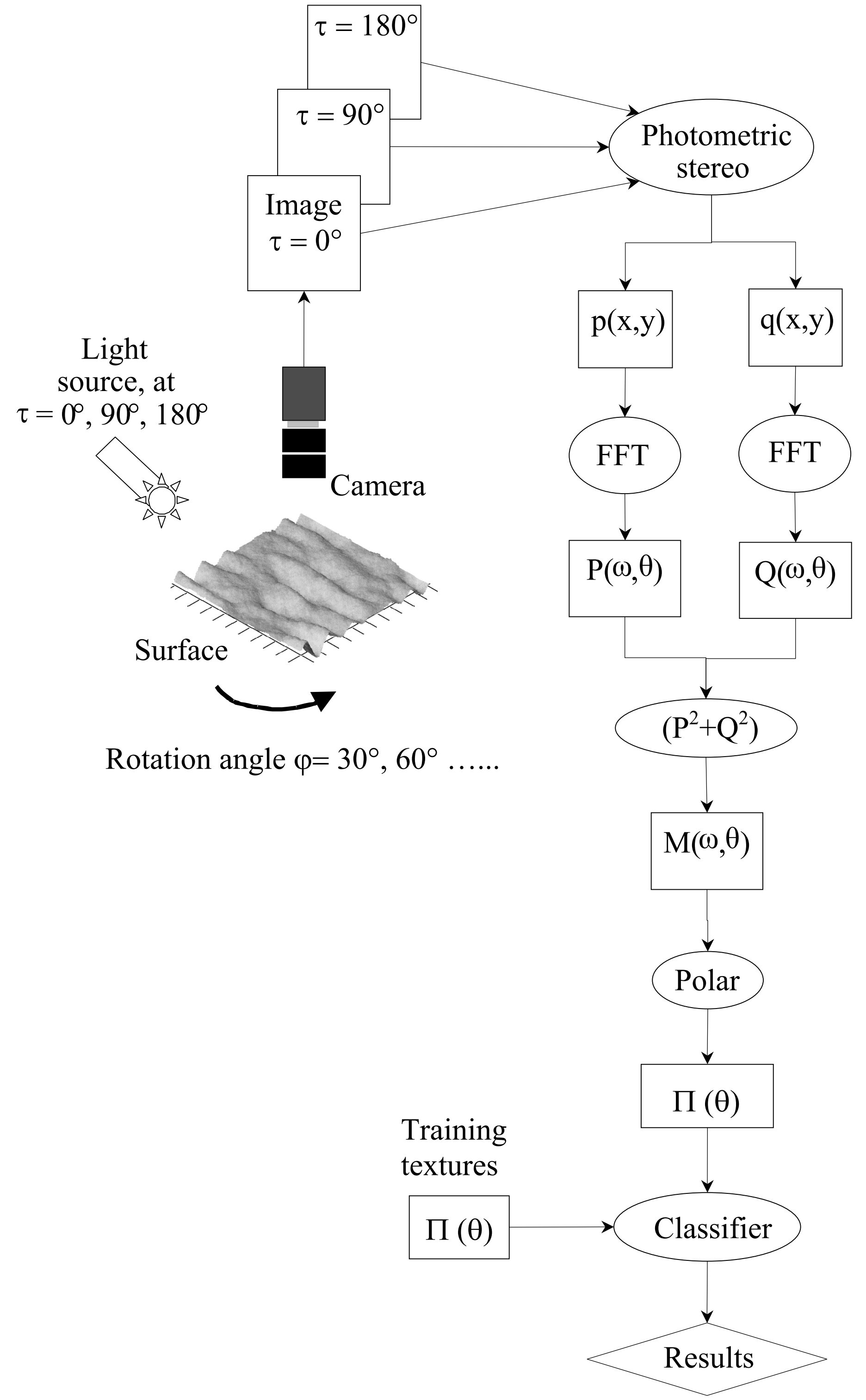

Figure 6. 22 The complete surface rotation invariant classification scheme

6.6.2 Texture Classification Scheme Using Image Information Only

In order to give the comparison of performance of *3D* surface rotation invariant classification using surface information (presented in *Figure 6. 22*) and image information respectively, we therefore present a classification scheme which only uses image information rather than surface information. The image-based texture classification for 3D surface is illustrated in *Figure 6. 23*.

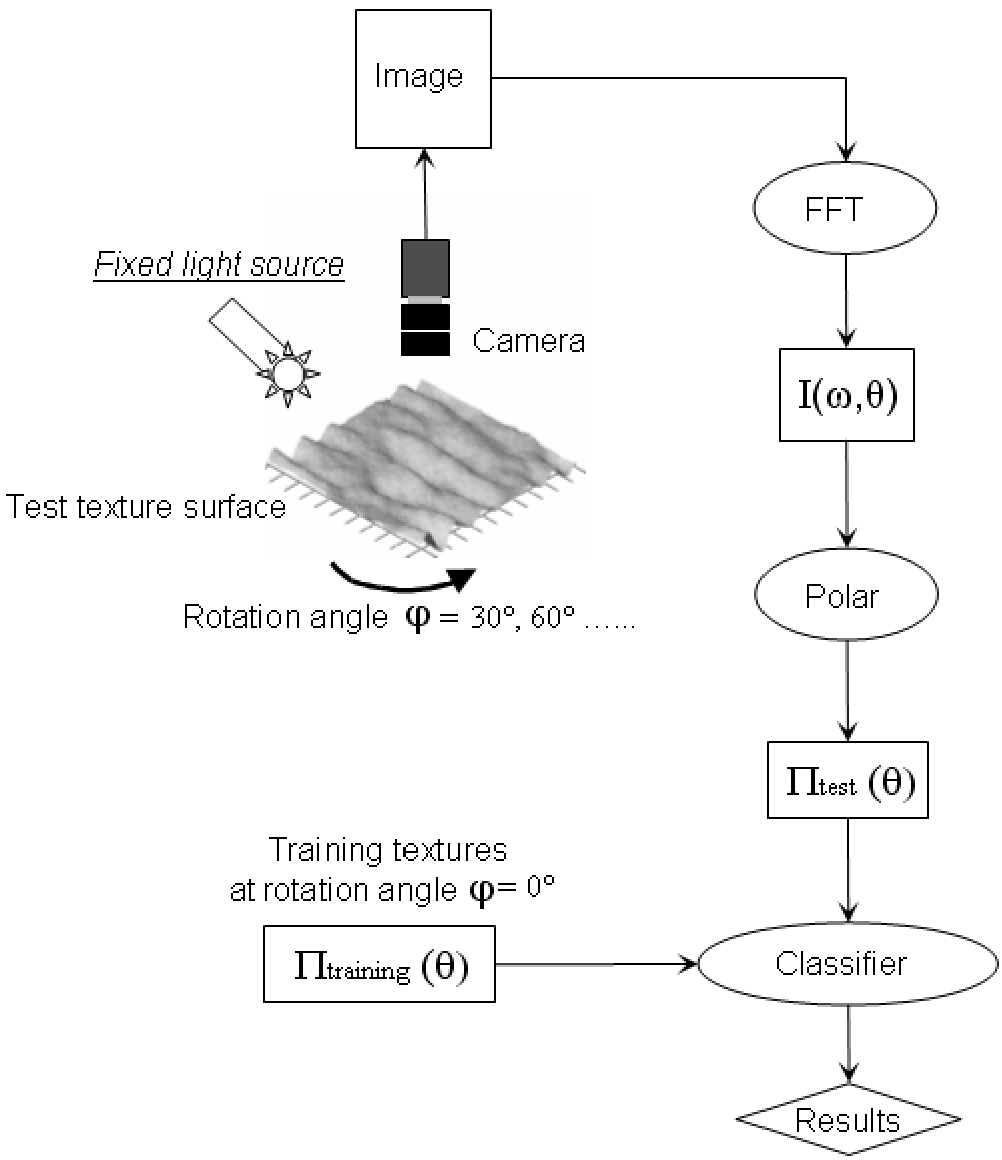

Figure 6. 23 The image-based texture classification for 3D surface

The process is as follows:

1. An image of the texture to be classified is captured by a digital camera which is fixed above the 3D rotated surface texture sample, while the illuminant tilt angle is fixed to *0°* during the whole experiment. Note that, for this image-based texture classification scheme, we only use a single image as the test set. On the other hand, for surface-based texture classification scheme, we use three input images to obtain the surface information by photometric stereo.
2. The captured single image is Fourier transformed into $I(\omega, \theta)$.
3. $I(\omega, \theta)$ is therefore processed to provide polar spectrum $\Pi_{test}(\theta)$.
4. The polar spectrum $\Pi_{test}(\theta)$ is compared with the polar spectra $\Pi_{training}(\theta)$ obtained from training images over a range of angular displacements (φ_{test}) using a sum of squared differences metric.
5. The total sum of squared difference metric calculated from step *4* and the best combination provides a classification decision based on the goodness-of-fit measurement.